Journal of Asian Ceramic Societies

Journal of Asian Ceramic Societies

journal homepage: www.elsevier.com/locate/jascer

Preparation and electrical properties of Li–Si–Al–O–N ceramics

Eiichirou Narimatsu*, Takashi Takeda, Toshiyuki Nishimura, Naoto Hirosaki

Sialon Group, Sialon Unit, National Institute for Materials Science, Namiki 1-1, Tsukuba, Ibaraki 305-0044, Japan

ARTICLE INFO

Article history:
Received 25 March 2013
Received in revised form 14 May 2013
Accepted 24 May 2013
Available online 14 June 2013

Keywords:
Nitrides
Electrical properties
$LiSi_2N_3$
Electronic conductivity
AFM

ABSTRACT

Ceramic samples were synthesized by hot pressing mixtures of Li_3N, Si_3N_4, AlN, Al_2O_3, and Li_2CO_3 with nominal compositions of $LiSi_{2-x}Al_xO_xN_{3-x}$ ($x = 0$–0.75) at 20 MPa and 1773–2073 K in a N_2 atmosphere of 0.10 MPa. The samples prepared with nominal compositions, $x = 0.25$ and 0.50, showed electronic conductivities of 2.2 and 4.2 S m^{-1} at room temperature with activation energies of 3.8 and 3.9 kJ mol^{-1}, respectively. Electronic conductive parts were detected in the sample of $x = 0.50$ by conductive atomic force microscopy (AFM). In this sample, a glassy thin layer, having a Si/Al atomic ratio of 3.8, was observed between the grains of $LiSi_{2-x}Al_xO_xN_{3-x}$ solid solution by high-resolution transmission electron microscopy (HRTEM). It was expected that the glassy phase of grain boundaries is an electronic conductive pathway besides the conductive parts observed by AFM.

1. Introduction

$LiSi_2N_3$ is known as a lithium ionic conductor [1–5]. The conductor is the stable compound against moisture and has a well-defined wurtzite-type structure (space group $Cmc2_1$) [4,5] that is isostructural with Li_2SiO_3. Regarding the practical use, $LiSi_2N_3$ is of particular interest because of its high stability against moisture. Recently, it was found that the electrical properties of $LiSi_2N_3$ change with the addition of doping additives such as B_2O_3, CaF_2, Y_2O_3, and Ca_3N_2 [2,3].

On the other hand, aluminum (Al) and oxygen (O) can substitute for silicon (Si) and nitrogen (N) in Si_3N_4. The incorporating Al and O into a Si_3N_4 matrix results in the family of solid solution ceramics known as SiAlONs [6–8]. It is known that SiAlON has improved oxidation resistance and corrosion resistance as compared to Si_3N_4 [7].

Upon Al and O substitution, Al^{3+} and O^{2-} may substitute for the Si^{4+} and N^{3-} ions of the $LiSi_2N_3$ structure, respectively. Also, Al and O may be segregated at grain boundaries and grain junctions in $LiSi_2N_3$ ceramics. However, to the best of our knowledge, there have been no detailed reports on the dependence of the electrical properties of $LiSi_2N_3$ ceramics on the substitution of aluminum (Al) and oxygen (O). Accordingly, the effects of Al and O substitution on the electrical properties of $LiSi_2N_3$ ceramics were investigated in this study. Interestingly, electronic conductivity of $LiSi_2N_3$ ceramics improved by the substitution of Al and O. Accordingly, the improvement of electronic conductivity is mainly discussed in this study.

2. Experimental procedure

$LiSi_2N_3$, and Al and O substituted $LiSi_2N_3$ were prepared by the reaction of Li_3N (>99% purity, Kojundo Chemical Lab. Co., Ltd., Saitama, Japan), α-Si_3N_4 (SN-E10, UBE Industries, Ube, Japan), AlN (E grade, Tokuyama Co., Ltd., Tokyo, Japan), Li_2CO_3 (99.99% purity, Kojundo), and Al_2O_3 (AKP-20, Sumitomo Chemical Co., Tokyo, Japan). The powders were mixed in stoichiometric compositions ($LiSi_{2-x}Al_xO_xN_{3-x}$ ($x = 0.10$–0.75)) using silicon nitride mortar in a dry state. Table 1 shows the compositions of the starting powders (A–G) used in this study. The mixed powder was placed in a 26-mm-diameter graphite mold and a thin BN plate was kept between the mold cap and the mixed powder to separate them. All the processes were carried out in a nitrogen-filled glove box. Hot pressing was performed at 1773 K, 1873 K, and 2073 K for 1 h under a pressure of 20 MPa in a N_2 atmosphere (0.10 MPa).

The crystal structure of each sample was determined by powder X-ray diffraction (XRD, D8 ADVANCE, Bruker, Karlsruhe, Germany) using Cu-Kα radiation. The densities of the samples were measured using Archimedes' method with distilled water as the immersion medium. The microstructures of the samples were observed by scanning electron microscopy (SEM, JSM-6700F, JEOL, Ltd., Tokyo, Japan). High-resolution transmission electron microscopy (HRTEM,

* Corresponding author. Tel.: +81 29 851 3354x8447; fax: +81 29 851 3613.
E-mail address: NARIMATSU.Eiichirou@nims.go.jp (E. Narimatsu).

Peer review under responsibility of The Ceramic Society of Japan and the Korean Ceramic Society.

Production and hosting by Elsevier

2187-0764 © 2013 The Ceramic Society of Japan and the Korean Ceramic Society. Production and hosting by Elsevier B.V. All rights reserved.
http://dx.doi.org/10.1016/j.jascer.2013.05.006

Table 1
Compositions, sintering temperatures, total conductivities at room temperature (298 K), electronic conductivities at room temperature (298 K), and activation energies of $LiSi_{2-x}Al_xO_xN_{3-x}$ (x = 0–0.75) samples (A–G), together with those of other lithium silicon nitride [1].

Sample	x in $LiSi_{2-x}Al_xO_xN_{3-x}$ starting powder	Sintering temperature(K)	Total conductivity σ_T (S m^{-1}) (298 K)	Electronic conductivity σ_e (S m^{-1}) (298 K)	Activation energy (kJ mol^{-1})
A	0	2073	3.1×10^{-9}	–	67
B	0	1773	3.9×10^{-10}	–	68
C	0.10	1773	2.2×10^{-10}	–	69
D	0.25	1773	4.9	4.2	3.8
E	0.50	1773	2.4	2.2	3.9
F	0.75	1773	4.2×10^{-10}	–	76
G	0.50	1873	1.5×10^{-11}	–	84
Ref. [1]	0	1475	1.9×10^{-8}	–	64

JEM-2100F; JEOL) was used to observe the grain boundaries. Composition analysis of the samples by energy-dispersive spectroscopy (EDS, JED-2300T; JEOL) in a device equipped with a field emission transmission electron microscope (FE-TEM, JEM-2100F; JEOL) was also performed.

Atomic force microscopy (AFM) measurements were performed in air using a S-image/NanoNaviReal (SII Nano Technology Inc., Chiba, Japan). Rh-coated Si probes were used for both morphological and conductive AFM (C-AFM) measurements. In C-AFM mode, C-AFM is able to image both the topography and the conductivity of the surface at the same time. The current flows between the cantilever and the sample allowing C-AFM mode to measure the surface conductivity of a sample.

Both sides of each sintered sample were polished to a 6 μm finish, and Au paste (Tanaka Kikinzoku, Tokyo, Japan) was applied to both sides of the sample by firing at 773 K for 30 min in N_2. Subsequently, a circular Pt electrode was attached to each side of the sample before it was mounted on the support tube in a ProboStat (NorECs AS., Oslo, Norway) measurement cell for electrochemical characterization (two-electrode measurements) [9,10]. Relatively strong spring loads were applied with alumina parts to hold the assembly together and to maintain contact between the sample and the electrodes. Each sample was heated to the measurement temperature in dry nitrogen and then maintained at this temperature for 0.5 h prior to the measurement of complex impedance using a Solartron 1260 impedance analyzer (Solartron, Farnborough, UK) equipped with a Solartron 1296 dielectric interface (Solartron). The measurement conditions were as follows: frequency range 0.10 Hz–10 MHz, applied voltage for impedance measurement 1 V, temperature range 298–690 K, flowing N_2 gas atmosphere.

Measurement of the dc polarization was also carried out by a potentiostat/galvanostat device (VersaSTAT4; Princeton Applied Research, Oak Ridge, Tennessee) to determine the electronic contribution to total conductivity of sintered sample using Au electrodes as blocking electrodes. A constant dc voltage of 1 V was applied to the hot-pressed samples at room temperature.

3. Results and discussion

All samples prepared with the starting compositions $LiSi_{2-x}Al_xO_xN_{3-x}$ (x = 0–0.75) ($LiSi_{2-x}Al_xO_xN_{3-x}$ (x = 0–0.75) samples (A–G)) were relatively stable in air at room temperature. After one-week exposure to air, their colors were not changed and there were few weight changes of the samples. The serial XRD patterns of $LiSi_{2-x}Al_xO_xN_{3-x}$ (x = 0–0.75, sintered at 1773 K and 1873 K) samples (B, D, E, F and G) are shown in Fig. 1. In Fig. 1, the XRD patterns of sample A and that of sample C were omitted, because they were similar to that of sample B. The XRD analysis indicates that $LiSi_2N_3$ is a primary phase in all samples. A small amount of $Li_2Al_2Si_3O_{10}$ phase exists as a secondary phase in the case of samples D, E, and G. A small amount of $Li_2Al_2Si_3O_{10}$ phase, $Li_5AlSi_2O_8$ phase, and unknown phase were detected by XRD analysis in the case of sample F. The diffraction patterns of the $LiSi_{2-x}Al_xO_xN_{3-x}$ (x = 0–0.75) samples (A–G) were similar to the JCPDS Powder Diffraction File Card 01-076-0517 (International Centre for Diffraction Data, Newtown Square, Pennsylvania) for crystal $LiSi_2N_3$ (an ordered variant of wurtzite (space group $Cmc2_1$)). The lattice parameters of each sample were obtained by fitting the powder XRD peak data using the $LiSi_2N_3$ crystal data [4] as an initial model and by using Jade 7 software (Rigaku, Tokyo, Japan). The lattice parameters a, b, and c increased just a little with increasing Al and O content in $LiSi_{2-x}Al_xO_xN_{3-x}$ (x = 0–0.75) starting powder. These results indicate that Al and O incorporated into $LiSi_2N_3$ lattice. Upon Al^{3+} and O^{2-} doping, Al^{3+} may substitute for the Si^{4+} and O^{2-} may substitute for the N^{3-} of the $LiSi_2N_3$ structure [11]. The radii of Si^{4+} and Al^{3+} for tetrahedral coordination (coordination number CN4) are 0.26 Å and 0.39 Å, respectively, and the radii of N^{3-} and O^{2-} for tetrahedral coordination (CN4) are 1.46 Å and 1.38 Å, respectively [12]. Thus, the incorporation of Al^{3+} (ionic radius: 0.39 Å (CN = 4)) into the smaller crystallographic site of Si^{4+} (ionic radius: 0.26 Å (CN = 4)) and the incorporation of O^{2-} (ionic radius: 1.38 Å (CN = 4)) into the larger crystallographic site of N^{3-} (ionic radius: 1.46 Å (CN = 4)) in the host $LiSi_2N_3$ lattice resulted in the lattice parameters being increased just a little. The little overall expansion of the lattice volume occurred due to the incorporation of Al^{3+} and O^{2-} ions. The total change in lattice volume is ~0.1% from x = 0 to 0.75.

On the other hand, the lattice parameters did not change with increasing sintering temperature in the case of $LiSi_{2-x}Al_xO_xN_{3-x}$

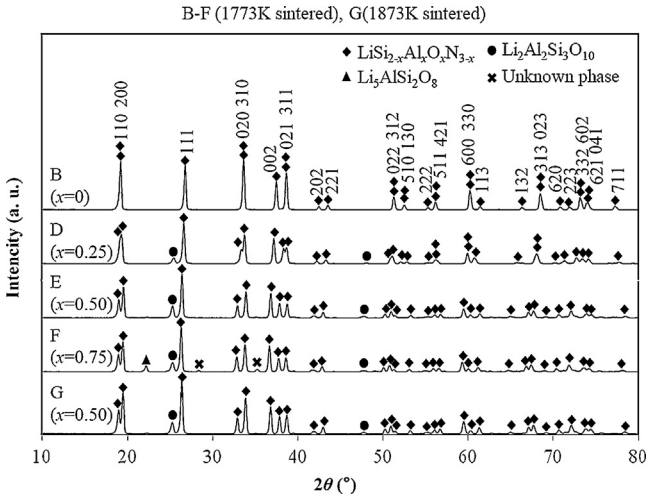

Fig. 1. XRD patterns of $LiSi_{2-x}Al_xO_xN_{3-x}$ (x = 0–0.75, sintered at 1773 K, 1873 K) samples (B, D, E, F and G).

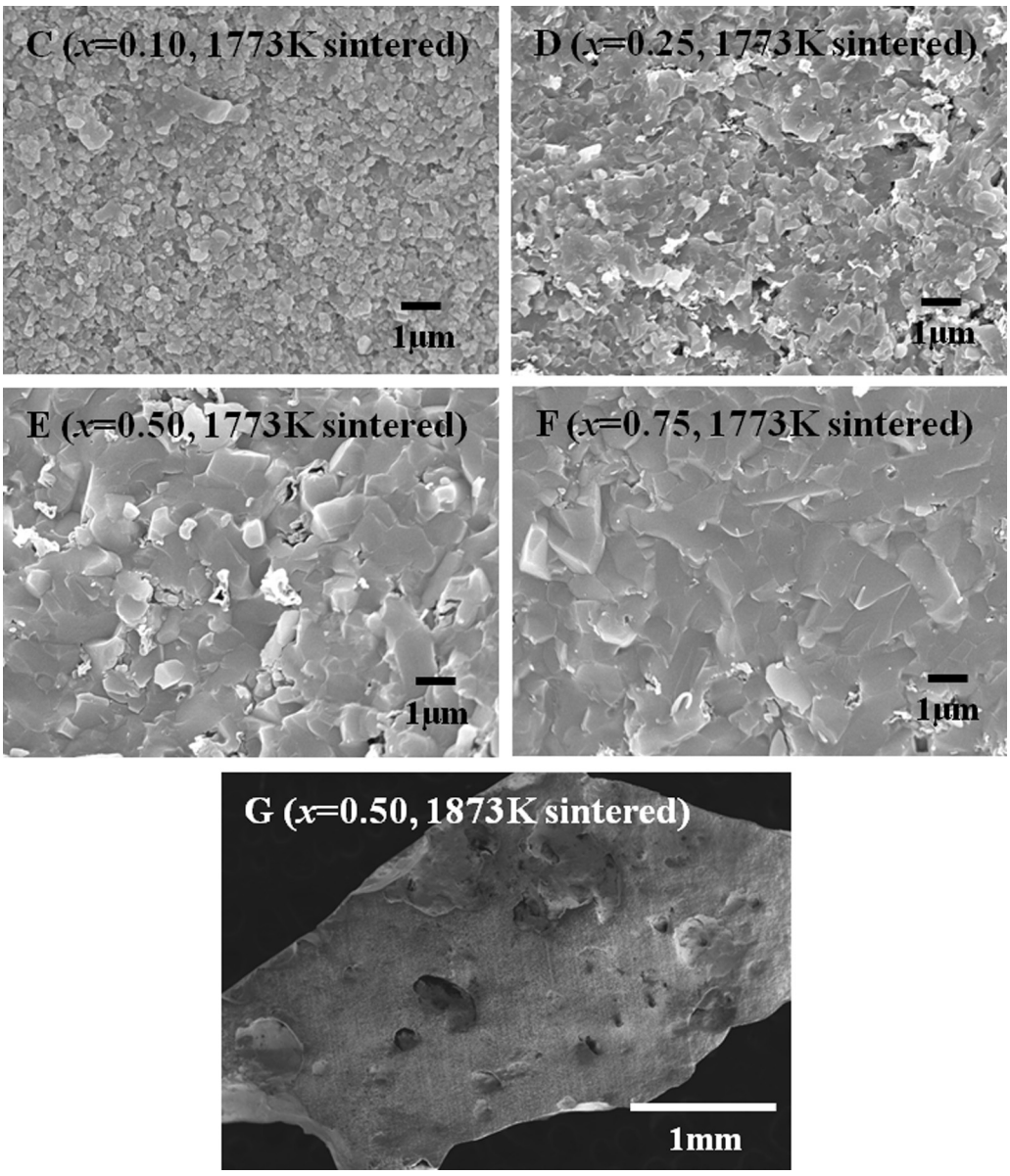

Fig. 2. SEM micrographs of fracture surface of sintered bodies of $LiSi_{2-x}Al_xO_xN_{3-x}$ samples.

($x = 0$) samples (A and B) and $LiSi_{2-x}Al_xO_xN_{3-x}$ ($x = 0.50$) samples (E and G).

The relative density of $LiSi_{2-x}Al_xO_xN_{3-x}$ ($x = 0$, sintered at 1773 K) sample (B) was 55% and that of $LiSi_{2-x}Al_xO_xN_{3-x}$ ($x = 0.10$–0.75, sintered at 1773 K) samples (C, D, E, and F) were about 95%. These results indicate that Al and O substitution promotes the densification of $LiSi_2N_3$ ceramics. On the other hand, in the case of $LiSi_{2-x}Al_xO_xN_{3-x}$ ($x = 0.50$), the relative density of sample G (sintered at 1873 K) (79%) was lower than that of sample E (sintered at 1773 K) (95%).

The micrographs of the as-hot-pressed materials are shown in Fig. 2. Grain size gradually increased with increasing x in $LiSi_{2-x}Al_xO_xN_{3-x}$ ($x = 0$–0.75) starting powder, and the grains were ~0.25–1.5 μm in diameter. No abnormal grain growth was observed, and the grains had an almost equiaxed form. The absence of residual porosity in the SEM images of materials C–F indicates that they were almost fully densified. On the other hand, sample G has many large pores. This is the reason why the density of sample G was lower than that of sample E. Grain boundary glassy phase shown below may be vaporized, because sintering temperature of sample G was higher than that of other samples.

To investigate the grain boundary chemistry in detail, HRTEM was used. Fig. 3 shows transmission electron microscopy (TEM) images of a grain boundary in the $LiSi_{2-x}Al_xO_xN_{3-x}$ ($x = 0.50$, sintered at 1773 K) sample (E) and $LiSi_{2-x}Al_xO_xN_{3-x}$ ($x = 0.50$, sintered at 1873 K) sample (G). The high-magnification images of both materials revealed that an intergranular glassy film existed at grain boundaries. The thicknesses of this film in sample E and sample G were almost 4 nm and 6 nm, respectively.

EDS elemental analysis using an FE-TEM with a focused electron beam size of ~1 nm was performed to examine the distribution of Al^{3+} and O^{2-} in $LiSi_{2-x}Al_xO_xN_{3-x}$ ($x = 0.50$, sintered at 1773 K) sample (E) and $LiSi_{2-x}Al_xO_xN_{3-x}$ ($x = 0.50$, sintered at 1873 K) sample (G). The spatial resolution available using the FE-TEM in this study was ~2–3 nm.

The EDS line analysis for grain boundary indicates that elemental Si, Al, O, and N are present in the grain boundary glassy phase. These results indicate that silicate-based Si–Al–O–N glassy phases

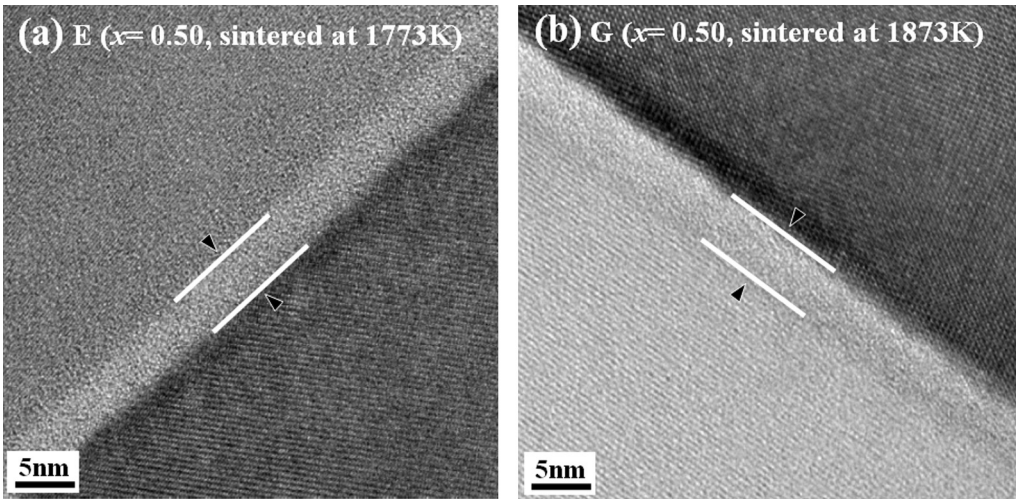

Fig. 3. High-resolution transmission electron microscopy image of a grain boundary in (a) $LiSi_{2-x}Al_xO_xN_{3-x}$ (x = 0.50, sintered at 1773 K) sample (E) and (b) $LiSi_{2-x}Al_xO_xN_{3-x}$ (x = 0.50, sintered at 1873 K) sample (G).

were formed at the grain boundaries of $LiSi_{2-x}Al_xO_xN_{3-x}$ (x = 0.50, sintered at 1773 K) sample (E) and $LiSi_{2-x}Al_xO_xN_{3-x}$ (x = 0.50, sintered at 1873 K) sample (G). EDS for grain boundaries between sample E and sample G was different. For example, Si/Al ratios of grain boundary glassy phases were 3.8 and 2.9 for sample E and sample G, respectively. These results show that grain boundary composition between sample E and sample G was different. Moreover, although lithium could not be detected by EDS, lithium content in the glassy phases between sample E and sample G may be also different.

The EDS point analysis for grain interior indicates that Al^{3+} and O^{2-} are present in the grain interior. This suggests that Al^{3+} and O^{2-} are incorporated into the $LiSi_2N_3$ host lattice. EDS for grain interiors between $LiSi_{2-x}Al_xO_xN_{3-x}$ (x = 0.50, sintered at 1773 K) sample (E) and $LiSi_{2-x}Al_xO_xN_{3-x}$ (x = 0.50, sintered at 1873 K) sample (G) was almost same. For example, Si/Al ratios of grain interiors were 3.7 and 3.7 for sample E and sample G, respectively. These results show that grain interior composition between sample E and sample G was nearly the same.

In typical complex impedance diagrams for $LiSi_{2-x}Al_xO_xN_{3-x}$ (x = 0.25 and 0.50, sintered at 1773 K) samples (D and E), no semicircular arc appeared and only inductive behavior was observed. The total conductivities of samples D and E were estimated from the intersection of the inductive line with the real axis.

Fig. 4 shows typical complex impedance diagrams for $LiSi_{2-x}Al_xO_xN_{3-x}$ (x = 0, sintered at 2073 K) sample (A), $LiSi_{2-x}Al_xO_xN_{3-x}$ (x = 0, 0.10, and 0.75, sintered at 1773 K) sample (B, C, and F), and $LiSi_{2-x}Al_xO_xN_{3-x}$ (x = 0.50, sintered at 1873 K) sample (G), respectively. One semicircular arc was observed for samples A and B. Two not well-resolved semicircular arcs were observed for samples C, F, and G. The total conductivities of samples A, B, C, F, and G were estimated from the intersections of impedance plot with the real axis (Z').

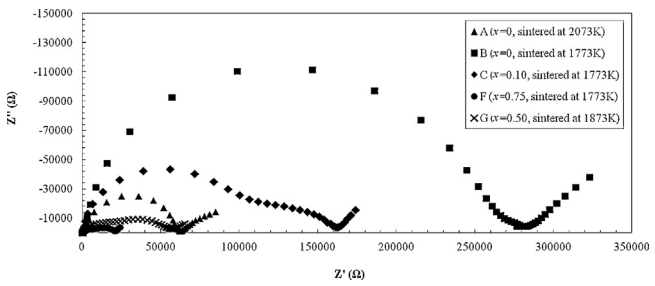

Fig. 4. Impedance spectra (recorded at 590 K in N_2) of $LiSi_{2-x}Al_xO_xN_{3-x}$ (x = 0, sintered at 2073 K) sample (A (▲)), $LiSi_{2-x}Al_xO_xN_{3-x}$ (x = 0, 0.10, and 0.75, sintered at 1773 K) samples (B (■), C (♦), and F (●)) and $LiSi_{2-x}Al_xO_xN_{3-x}$ (x = 0.50, sintered at 1873 K) sample (G (×)).

A constant voltage of 1 V was applied to $LiSi_{2-x}Al_xO_xN_{3-x}$ (x = 0.25 and 0.50, sintered at 1773 K) samples (D and E) and $LiSi_{2-x}Al_xO_xN_{3-x}$ (x = 0, sintered at 2073 K) sample (A), $LiSi_{2-x}Al_xO_xN_{3-x}$ (x = 0, 0.10, and 0.75, sintered at 1773 K) samples (B, C, and F) and $LiSi_{2-x}Al_xO_xN_{3-x}$ (x = 0.50, sintered at 1873 K) sample (G) for 1800 s using Au blocking electrodes to determine the electronic contribution.

In the case of samples D and E, these samples retain the constant high current density (819–2183 A m^{-2}) with time and exhibit the electronic conductivity of 2.2–4.2 S m^{-1}. The electronic conductivities are in good agreement with the total conductivities of 2.4–4.9 S m^{-1} which were calculated from the resistances obtained by the ac impedance technique using Au as blocking electrodes. These results indicate that large part of the conductivity of the samples D and E is due to electronic conduction.

The samples A, B, C, F and G were initially polarized, and then the current densities drastically decreased within 0.001 s. The dc conductivities of samples A, B, C, F, and G obtained using the steady currents after polarization were less than 10^{-16} S m^{-1}. The difference between ac conductivity and dc conductivity indicates the difference between total conductivity (ionic conductivity + electronic conductivity) and electronic conductivity. The total conductivities of samples A, B, C, F and G were about 5 orders of magnitude higher than the electronic conductivities. These results indicate that the electronic conductivities of samples A, B, C, F and G were negligibly small. Thus, most of the conductivities of the samples A, B, C, F and G are caused by the migration of lithium ions.

Fig. 5 shows the temperature dependences of the total conductivity for all the $LiSi_{2-x}Al_xO_xN_{3-x}$ (x = 0–0.75) samples (A–G) considered in this study. Table 1 summarizes the total conductivities at room temperature (298 K), electronic conductivities at room temperature (298 K), and activation energies of conduction of the $LiSi_{2-x}Al_xO_xN_{3-x}$ (x = 0–0.75) samples (A–G), together with those of other lithium silicon nitride [1]. The total conductivities at 298 K for samples A, B, C, F, and G were estimated by extrapolating the lines representing conductivity shown in Fig. 5 to 298 K.

The activation energies for conduction of $LiSi_{2-x}Al_xO_xN_{3-x}$ (x = 0, sintered at 1773 K and 2073 K) samples (A and B) and that of

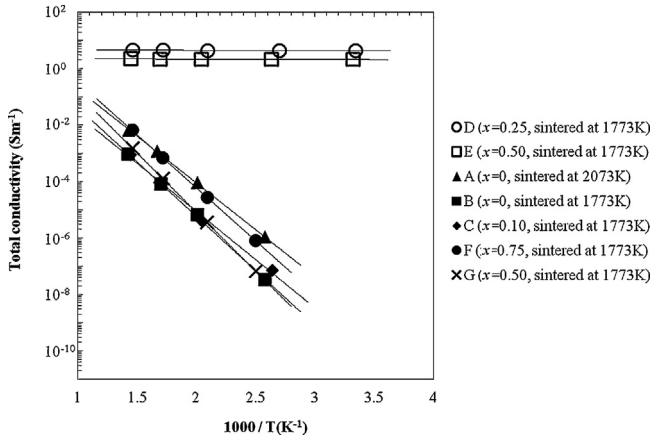

Fig. 5. Temperature dependences of total conductivities of $LiSi_{2-x}Al_xO_xN_{3-x}$ ($x = 0$, sintered at 2073 K) sample (A (▲)), $LiSi_{2-x}Al_xO_xN_{3-x}$ ($x = 0$, 0.10, 0.25, 0.50 and 0.75, sintered at 1773 K) samples (B (■), C (♦), D (○), E (□), and F (●)) and $LiSi_{2-x}Al_xO_xN_{3-x}$ ($x = 0.50$, sintered at 1873 K) sample (G (×)).

$LiSi_{2-x}Al_xO_xN_{3-x}$ ($x = 0.10$, sintered at 1773 K) sample (C) were 67, 68, and 69 kJ mol^{-1}, respectively. Yamane et al. reported the preparation and ionic conductivity of $LiSi_2N_3$ [1]. The activation energy for conduction of their $LiSi_2N_3$ was 64 kJ mol^{-1}. The activation energies for conduction of samples A, B, and C were comparable to that of Yamane et al.'s material, because their phases were almost same. The activation energies for conduction of $LiSi_{2-x}Al_xO_xN_{3-x}$ ($x = 0.75$, sintered at 1773 K) sample (F) and $LiSi_{2-x}Al_xO_xN_{3-x}$ ($x = 0.50$, sintered at 1873 K) sample (G) were 76 and 84 kJ mol^{-1}, respectively. The activation energies of sample F and sample G were 10–20 kJ/mol higher than that of samples A, B, and C. Sample F has many other impurity phases as shown in Fig. 1. These impurity phases block the migration of lithium ions. The activation energy (84 kJ mol^{-1}) of sample G was the highest among the samples prepared in this study. Sample G has many large pores as shown in Fig. 2. These pores block the migration of lithium ions.

The activation energies (3.8–3.9 kJ mol^{-1}) for conduction of $LiSi_{2-x}Al_xO_xN_{3-x}$ ($x = 0.25$ and 0.50, sintered at 1773 K) samples (D and E) were the lowest among the samples prepared in this study, because of their high electronic conductivity. The activation energies of samples D and E were 60–80 kJ/mol lower than that of samples A, B, C, F, and G. The total conductivities at room temperature (298 K) of samples D and E were high (2.4–4.9 S m^{-1}), because of their high electronic conductivity. At 298 K, the electronic conductivities of samples D and E achieved 2.2–4.2 S m^{-1}.

To confirm the existence of percolated electronic conduction pathways in these electronic conductive samples, conducting AFM was performed. Fig. 6 shows (a) AFM surface morphology image of the electronic conductive $LiSi_{2-x}Al_xO_xN_{3-x}$ ($x = 0.50$, sintered at

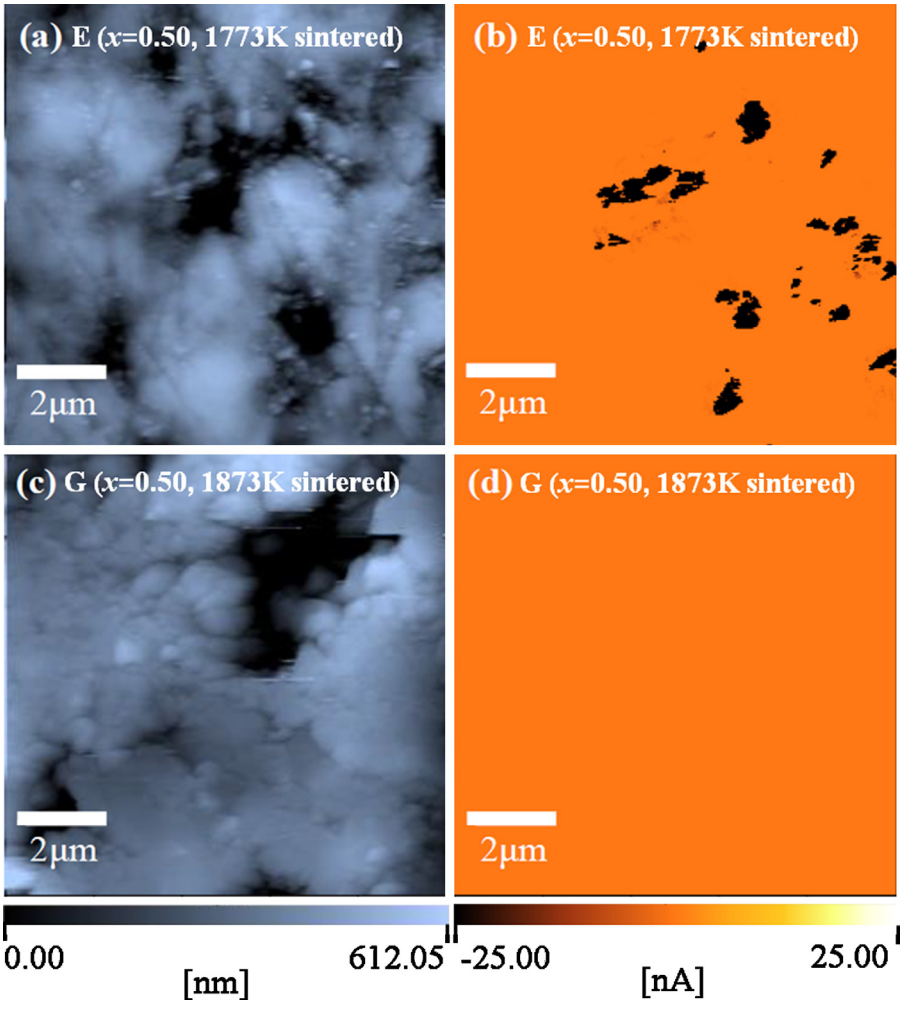

Fig. 6. (a) AFM surface morphology image of the electronic conductive $LiSi_{2-x}Al_xO_xN_{3-x}$ ($x = 0.50$, sintered at 1773 K for 1 h) sample (E), (b) the corresponding current map for sample E (bias voltage −5 V), (c) AFM surface morphology image of the non-electronic conductive $LiSi_{2-x}Al_xO_xN_{3-x}$ ($x = 0.50$, sintered at 1873 K for 1 h) sample (G), and (d) the corresponding current map for sample G (bias voltage −5 V).

1773 K 1 h) sample (E), (b) the corresponding current map for sample E (bias voltage −5 V), (c) AFM surface morphology image of the non-electronic conductive $LiSi_{2-x}Al_xO_xN_{3-x}$ ($x = 0.50$, sintered at 1873 K for 1 h) sample (G), and (d) the corresponding current map for sample G (bias voltage −5 V). As shown in Fig. 6(b), in the case of sample E which shows electronic conductivity, some conductive areas appeared. Because of the C-AFM geometry employed, in which the current flows between the tip probe and the remote surface electrode, the formation of a conducting network is evident. This result indicates that a conducting network is formed in sample E. On the other hand, as shown in Fig. 6(d), conductive area did not appear in the case of sample G which did not show electronic conductivity.

In this study, electronic conductive $LiSi_{2-x}Al_xO_xN_{3-x}$ ($x = 0.25$ and 0.50, sintered at 1773 K) samples (D and E) have small amount of lithium alumino-silicate ($Li_2Al_2Si_3O_{10}$) secondary phase. However, lithium alumino-silicate phase has low ionic conductivity (2.8×10^{-7} S m^{-1} at 398 K) and high activation energy (66–100 kJ mol^{-1}) [13,14]. Therefore, we believe that the electronic conductivities of the samples D and E are caused by the $LiSi_{2-x}Al_xO_xN_{3-x}$ grains or the grain boundary (Li)–Si–Al–O–N glassy phases.

Moreover, XRD patterns between electronic conductive sample E and non-electronic conductive sample G were almost same, as shown in Fig. 1. Also, as mentioned above, the grain interior compositions between samples E and G were almost same. On the other hand, the grain boundary glassy phase compositions between samples E and G were different. These results suggest that the difference of conductivities between sample E and sample G could be due to the difference of grain boundary glassy phase compositions between sample E and sample G. Also, as shown in Fig. 3, the grain boundary glassy phase existed as a continuous intergranular film between grains. The continuous glassy phase is a common feature of the liquid-phase sintered ceramics using Si_3N_4 as starting powder [15,16]. The continuous glassy phase has an equilibrium thickness and cannot be removed easily [16]. In this context, we can assume that the continuous glassy phases shown in Fig. 3 form a percolated network in $LiSi_{2-x}Al_xO_xN_{3-x}$ samples. Judging from these results, continuous (Li)–Si–Al–O–N glassy phases may be electronic conductive percolated pathways in samples D and E which shows electronic conductivity. The dimension of the grain boundary glassy phases shown in Fig. 3 is different from that of the conductive areas shown in Fig. 6(b). The conductive areas shown in Fig. 6(b) may contain a lot of electronic conductive grain boundary glassy phases.

If both the $LiSi_{2-x}Al_xO_xN_{3-x}$ grains and the grain boundary (Li)–Si–Al–O–N glassy phases have electronic conductivity in electronic conductive samples, almost all parts of sample must have electronic conductivity. However, as shown in Fig. 6(b), conductive areas were limited in some areas. Thus, there is little possibility that both the $LiSi_{2-x}Al_xO_xN_{3-x}$ grains and the grain boundary (Li)–Si–Al–O–N glassy phases have electronic conductivity in electronic conductive samples.

4. Conclusions

In this study, the effect of the substitution of Al and O on the electrical properties of $LiSi_2N_3$ was studied. The activation energies for conduction of $LiSi_{2-x}Al_xO_xN_{3-x}$ ($x = 0.25$ and 0.50, sintered at 1773 K) samples were very low (3.8–3.9 kJ mol^{-1}). The total conductivities at room temperature (298 K) of these samples were high (2.4–4.9 S m^{-1}) because of its high electronic conductivity. At 298 K, the electronic conductivities of $LiSi_{2-x}Al_xO_xN_{3-x}$ ($x = 0.25$ and 0.50, sintered at 1773 K) samples achieved 2.2–4.2 S m^{-1}.

Conducting AFM results indicated that some conductive areas existed in sample which shows electronic conductivity. It was expected that a percolated (Li)–Si–Al–O–N glassy phase network is the electronic conductive pathway in samples which shows electronic conductivity.

References

[1] H. Yamane, S. Kikkawa and M. Koizumi, Solid State Ionics, 25, 183–191 (1987).
[2] E. Narimatsu, Y. Yamamoto, T. Nishimura and N. Hirosaki, J. Ceram. Soc. Jpn., 118, 837–841 (2010).
[3] E. Narimatsu, Y. Yamamoto, T. Takeda, T. Nishimura and N. Hirosaki, J. Mater. Res., 26, 1133–1142 (2011).
[4] J. David, Y. Laurent, J.P. Charlot and J. Lang, Bull. Soc. Fr. Mineral. Cristallogr., 96, 21–24 (1973).
[5] M. Orth and W. Schnick, Z. Anorg. Allg. Chem., 625, 1426–1428 (1999).
[6] M. Mitomo and A. Ishida, J. Eur. Ceram. Soc., 19, 7–15 (1999).
[7] J. Briggs, Mater. Res. Bull., 12, 1047–1055 (1977).
[8] Y.Q. Li, N. Hirosaki, R.J. Xie, T. Takeda and M. Mitomo, J. Solid State Chem., 181, 3200–3210 (2008).
[9] P.I. Dahl, R. Haugsrud, H.L. Lein, T. Grande, T. Norby and M. Einarsrud, J. Eur. Ceram. Soc., 27, 4461–4471 (2007).
[10] T. Norby and M. Hartmanova, Solid State Ionics, 67, 57–64 (1993).
[11] Y.Q. Li, N. Hirosaki, R.J. Xie, T. Takeka and M. Mitomo, J. Solid State Chem., 182, 301–311 (2009).
[12] R.D. Shannon, Acta Crystallogr., A32, 751–767 (1976).
[13] R.T. Johnson Jr., B. Morosin, M.L. Knotek and R.M. Biefeld, Phys. Lett., 54A, 403–404 (1975).
[14] Y. Fukushige, T. Okamoto and K. Shimada, Yogyo Kyokai Shi, 80, 503–505 (1972).
[15] S. Hampshire, J. Eur. Ceram. Soc., 32, 1925–1932 (2012).
[16] D.R. Clarke, J. Am. Ceram. Soc., 70, (1) 15–22 (1987).